Petroleum Science 20 (2023) 2759–2772

Contents lists available at ScienceDirect

Petroleum Science

journal homepage: www.keaipublishing.com/en/journals/petroleum-science

Original Paper

Finite-difference modeling of Maxwell viscoelastic media developed from perfectly matched layer

Ruo-Long Song

College of Physics, Jilin University, Changchun, 130012, Jilin, China

ARTICLE INFO

Article history:
Received 14 June 2022
Received in revised form
3 November 2022
Accepted 12 April 2023
Available online 15 April 2023

Edited by Jie Hao

Keywords:
Finite difference
Viscoelastic model
Nonsplitting perfectly matched layer

ABSTRACT

In numerical simulation of wave propagation, both viscoelastic materials and perfectly matched layers (PMLs) attenuate waves. The wave equations for both the viscoelastic model and the PML contain convolution operators. However, convolution operator is intractable in finite-difference time-domain (FDTD) method. A great deal of progress has been made in using time stepping instead of convolution in FDTD. To incorporate PML into viscoelastic media, more memory variables need to be introduced, which increases the code complexity and computation costs. By modifying the nonsplitting PML formulation, I propose a viscoelastic model, which can be used as a viscoelastic material and/or a PML just by adjusting the parameters. The proposed viscoelastic model is essentially equivalent to a Maxwell model. Compared with existing PML methods, the proposed method requires less memory and its implementation in existing finite-difference codes is much easier. The attenuation and phase velocity of P- and S-waves are frequency independent in the viscoelastic model if the related quality factors (Q) are greater than 10. The numerical examples show that the method is stable for materials with high absorption ($Q = 1$), and for heterogeneous media with large contrast of acoustic impedance and large contrast of viscosity.

1. Introduction

In finite-difference time-domain (FDTD) method, absorbing boundary conditions (ABCs) are important for simulating waves propagation in unbounded media using truncated mesh. Considerable efforts have been made to develop various ABCs, see the reviews in Komatitsch and Martin (2007). The perfectly matched layer (PML), has proven to be the most robust and efficient technique for absorbing outgoing waves. The original (or standard) PML was first introduced by Bérenger (1994) as a material ABC for electromagnetic waves simulation. Then it was applied to simulations of acoustic and elastic wave propagation problems (Chew and Liu, 1996; Liu and Tao, 1997; Collino and Tsogka, 2001; Zeng et al., 2001; Liu and Sinha, 2003). The wave equations for PML can be formulated with complex stretched coordinates (Chew and Weedon, 1994). These equations involve convolution operators in the time domain. The traditional implementation of PML (Bérenger, 1994; Chew and Liu, 1996), which is referred to as SPML, spilts the fields in PML region to avoid convolutional operations. However, two different sets of equations must be solved due to field splitting. To avoid field splitting, Wang and Tang (2003) proposed a nonsplitting PML method (NPML) by replacing the convolutional integral with an explicit time-marching scheme based on trapezoidal integration rule. Ramadan (2003) proposed another unsplit-field implementation of PML for Maxwell's equations, which used auxiliary differential equations (ADE) to update auxiliary memory variables, namely ADE-PML.

Nevertheless, the standard PML was weakly causal (Teixeira and Chew, 1999) and ineffective at absorbing evanescent waves (Bérenger, 1997, 1998, 1999) and grazing-incidence waves (Komatitsch and Martin, 2007). Kuzuoglu and Mittra (1996) introduced a strictly causal form of the PML by shifting the frequency-dependent pole off the real axis, which was then referred to as complex frequency-shifted PML (CFS-PML) (Bérenger, 2002a, 2002b). The CFS-PML originally was implemented in a split-field form. Three auxiliary memory variables are needed for each derivative. Roden and Gedney (2000) presented an efficient implementation of CFS-PML for Maxwell's equations, in which the convolutional operations were performed recursively using the recursive convolution method. They called their method as convolutional PML (CPML) and applied it to study electromagnetic

E-mail address: songrl@jlu.edu.cn.

https://doi.org/10.1016/j.petsci.2023.04.009

scattering by a highly elongated plate. Then CPML was adapted to the seismic wave equation (Komatitsch and Martin, 2007; Martin et al., 2008). The CPML introduced memory variables to avoid explicitly storing all the past states in convolution operation. Drossaert and Giannopoulos (2007) introduced a nonsplitting implementation of standard PML and CFS-PML based on the trapezoidal integration rule. This method was called the recursive integration PML (RIPML). Martin et al. (2010) and Zhang and Shen (2010) proposed the ADE-PML implementation for CFS-PML. Martin et al. (2010) demonstrated that the ADE-PML formulation can be extended to high-order schemes in time, which implies that it can be made more accurately. However, for a second-order time scheme, the time-marching equations of ADE-PML have the same form as the CPML formulations given by Komatitsch and Martin (2007).

All the above-mentioned implementations of standard PML and CFS-PML are developed for elastic materials. Real materials are not perfectly elastic. Both attenuation and dispersion can be observed when waves propagate in real materials. These behaviors can be described by using viscoelastic constitutive equations based on mechanical models consisting of two basic elements: springs and dashpots. The weightless springs represent the elastic solid, and the dashpots, consisting of loosely fitting pistons in cylinders filled with a viscous fluid, represent the viscous dissipation. Several viscoelastic models have been developed. The Maxwell model (Maxwell, 1867) is a series combination of a spring and a dashpot, so it is more appropriate for representing a viscoelastic fluid. The Kelvin–Voigt model (Kelvin and Thomson, 1875) consists of a spring and a dashpot connected in parallel. The creep function of Kelvin–Voigt model lacks the instantaneous response of real solids. The Zener model (Zener, 1948) or standard linear solid, which consists of a series combination of a spring and a Kelvin–Voigt model, gives a more realistic representation of real materials. There is one peak in the dissipation factor versus frequency curve for Zener model. The Burgers model is formed with a series connection of a Kelvin–Voigt element and a Maxwell element (Carcione, 2015). To broaden the peak of dissipation factor, Liu et al. (1976) introduced generalized Zener model by combining a finite number of relaxation mechanisms or a continuous distribution of relaxation mechanisms. Each relaxation mechanism represents a single Zener model. The generalized Zener model is equivalent to a parallel system with many Zener elements connected in parallel. Extensive reviews on viscoelastic models can be found in Chapter 2 in Carcione (2015).

The stress-strain relation is usually formulated as convolution operator in viscoelastic materials (Liu et al., 1976; Kjartansson, 1979). However, this representation is intractable in FDTD. Considerable efforts have been made in the development of various approaches to incorporate attenuation into FDTD computations of wave fields in viscoelastic media. Fan et al. (2016) reviewed these methods and divided them into two categories. In the first category, the convolution in the time-domain was reformulated in terms of fractional derivatives, which were computed with Grünwald-Letnikov approximation and central-difference approximation (Carcione et al., 2002; Carcione, 2009; Treeby and Cox, 2010; Zhu and Carcione, 2014; Zhu and Harris, 2014). In the second category, memory variables were introduced, so the convolution was replaced by a set of coupled first-order linear differential equations (Day and Minster, 1984; Emmerich and Korn, 1987; Carcione et al., 1988a, b; Robertsson et al., 1994; Blanch et al., 1995; Fabien-Ouellet et al., 2017). The differential equation for each memory variable represents a relaxation mechanism. The frequency dependent complex moduli, attenuation and phase velocity are determined by the relaxation times. Then, the desired attenuation property, such as constant quality factor material (Blanch et al., 1995), can be obtained by choosing the number of relaxation mechanism and their relaxation time. The computational costs and memory requirements depend on the numbers of relaxation mechanism. In addition to these methods, Dhemaied et al. (2011) proposed the ADE implementation of FDTD modeling of two-dimensional (2D) seismic wave propagation in viscoelastic media, similar to the ADE implementation of the PML proposed by Ramadan (2003). Martin et al. (2019) made a 3D extension of the ADE implementation proposed by Dhemaied et al. (2011). When compared with the memory variable technique, the ADE implementation is more flexible at the cost of requiring a bit more variables (additional strain components).

When the standard PML or CFS-PML is applied to viscoelastic materials, new problems arise. Liu and Tao (1997) applied SPML to absorptive fluid media. They found that an additional term involving time-integrated pressure field had to be introduced to account for the coupling between the loss from the PML and the material absorption. Martin and Komatitsch (2009) applied CPML to viscoelastic media. They also found that additional variables and additional differential equations must be introduced in the formulation. The number of arrays in the PML regions for a 3D problem is 19 for elastic material, and 39 for viscoelastic material. In CPML technique, the required memory for viscoelastic material is doubled. Liu et al. (2018) followed an approach similar to Martin and Komatitsch (2009) for simulating seismic wave propagation in viscoelastic media. Dhemaied et al. (2011) combined the ADE implementation for viscoelastic media and the CPML technique, where a total of 16 arrays were required for 2D cases. Martin et al. (2019) applied the ADE method for both viscoelastic media and PML. The formulations of their ADE system indicate that they also need 39 arrays for 3D cases.

Both viscoelastic medium and PML attenuate waves. Komatitsch and Martin (2007) noted that the idea of using memory variables in PML was rather similar to that used in numerical modeling of seismic wave propagation in viscoelastic materials. Carcione and Kosloff (2013) represented the PML kernels with viscoelastic mechanical models. They demonstrated that the SPML method was based on a Maxwell viscoelastic model, and the CPML method was based on the Zener viscoelastic model.

Considering that the PML is equivalent to the damping kernel of viscoelastic model, in this work, based on NPML method (Wang and Tang, 2003), I propose a set of wave equations that provides a unified basis for both viscoelastic materials and the PML regions. The equations are easy to be implemented in existing codes, and computationally economical and stable. This work is organized as follow. In the first part of this work I review the NPML method, introduce a viscoelastic model, and investigate the attenuation and dispersion in the model. Then I propose a unified set of equations for viscoelastic materials and PML regions and demonstrate their implementation in FDTD. In the second part, using numerical examples, I verify the attenuation in materials with various viscosities, and finally I apply the new method to simulate leaky Lamb wave propagation in multi-layered structure.

2. Formulations

In this section, I introduce a viscoelastic model by modifying PML formulation, and illustrate its finite difference implementation in a 2D Cartesian geometry. The formulations for 3D geometry are given in the APPENDIX.

2.1. Nonsplitting perfectly matched layer

The NPML simplifies the numerical implementation of the split-field PML (Chew and Liu, 1996) without sacrificing the accuracy. I

use 2D Cartesian coordinates to repeat the NPML method for the convenience of the following discussions. More details can be found in Wang and Tang (2003).

For the two-dimensional case, the constitutive relations and motion equations of an isotropic elastic material are

$$\begin{cases} \partial_t \tau_{xx} = (\lambda + 2\mu)\partial_x v_x + \lambda \partial_z v_z \\ \partial_t \tau_{zz} = \lambda \partial_x v_x + (\lambda + 2\mu)\partial_z v_z \\ \partial_t \tau_{xz} = \mu(\partial_x v_z + \partial_z v_x) \end{cases}, \tag{1}$$

$$\begin{cases} \rho \partial_t v_x = \partial_x \tau_{xx} + \partial_z \tau_{xz} \\ \rho \partial_t v_z = \partial_x \tau_{xz} + \partial_z \tau_{zz} \end{cases} \tag{2}$$

where ∂_m denotes the spatial derivative along the m-direction, $m = x, z$; v_x, v_z are particle-velocity components; τ_{xx}, τ_{zz}, τ_{xz} are stress components; ρ is the density, λ and μ are the Lamé coefficients.

The PML is introduced by a coordinate stretching of spatial coordinates to the complex-variable domain, which in frequency domain can be expressed as

$$\partial_m \rightarrow \frac{1}{s_m}\partial_m, \quad s_m = 1 + \frac{\Omega_m}{i\omega} \ (m = x, z) \tag{3}$$

where Ω_m are chosen as (Chew and Liu, 1996)

$$\Omega_m(m) = \frac{v_P \beta}{L}\left[\frac{1}{4}\frac{m}{L} + \frac{3}{4}\left(\frac{m}{L}\right)^2\right], \quad m = x, z, \tag{4}$$

where L is the width of the PML region in meter, v_P is the P-wave velocity of medium in the PML region, and β is a predefined level of wave absorption.

Assuming the $e^{i\omega t}$ convention, transforming Eqs. (1) and (2) to the frequency domain, and stretching the spatial coordinates give

$$\begin{cases} i\omega T_{xx} = (\lambda + 2\mu)\dfrac{i\omega}{\Omega_x + i\omega}\partial_x V_x + \lambda \dfrac{i\omega}{\Omega_z + i\omega}\partial_z V_z \\ i\omega T_{zz} = \lambda \dfrac{i\omega}{\Omega_x + i\omega}\partial_x V_x + (\lambda + 2\mu)\dfrac{i\omega}{\Omega_z + i\omega}\partial_z V_z \\ i\omega T_{xz} = \mu \dfrac{i\omega}{\Omega_x + i\omega}\partial_x V_z + \mu \dfrac{i\omega}{\Omega_z + i\omega}\partial_z V_x \end{cases}, \tag{5}$$

$$\begin{cases} i\omega \rho V_x = \dfrac{i\omega}{\Omega_x + i\omega}\partial_x T_{xx} + \dfrac{i\omega}{\Omega_z + i\omega}\partial_z T_{xz} \\ i\omega \rho V_z = \dfrac{i\omega}{\Omega_x + i\omega}\partial_x T_{xz} + \dfrac{i\omega}{\Omega_z + i\omega}\partial_z T_{zz} \end{cases} \tag{6}$$

where V_x, V_z, T_{xx}, T_{zz} and T_{xz} are the velocity and stress fields in the frequency domain.

Inversing Fourier transform Eqs. (5) and (6) gives the set of NPML equations in time domain. By sake of simplicity, I take the first one in Eq. (6) for example,

$$\rho \partial_t v_x = (1 + \psi_x)\partial_x \tau_{xx} + (1 + \psi_z)\partial_z \tau_{xz}, \tag{7}$$

where $\psi_m = -\Omega_m e^{-\Omega_m t} * \ (m = x, z)$ are convolutional operators. The NPML equations reduce automatically to the original wave equations when Ω_x and Ω_z vanish.

The convolution integrals are approximated with the trapezoidal rule. By applying second order time update, Eq. (7) can be written as

$$v_x^{n+1/2} = v_x^{n-1/2} + \frac{\Delta t}{\rho}\left[\left(\partial_x \tau_{xx}^n + P_{xx}^n\right) + \left(\partial_z \tau_{xz}^n + P_{xz}^n\right)\right], \tag{8}$$

where P_{xx}^n, P_{xz}^n are the memory variables. These memory variables can be updated in each iteration of the time loop using

$$P_{xx}^n = e^{-\Omega_x \Delta t} P_{xx}^{n-1} - \frac{1}{2}\Omega_x \Delta t\left(e^{-\Omega_x \Delta t}\partial_x \tau_{xx}^{n-1} + \partial_x \tau_{xx}^n\right), \tag{9}$$

$$P_{xz}^n = e^{-\Omega_z \Delta t} P_{xz}^{n-1} - \frac{1}{2}\Omega_z \Delta t\left(e^{-\Omega_z \Delta t}\partial_z \tau_{xz}^{n-1} + \partial_z \tau_{xz}^n\right). \tag{10}$$

The number of memory variables is the same as the number of the spatial derivatives in Eqs. (5) and (6). A total of 8 memory variables are needed in the PML regions. In addition to the 5 components of stress and velocity, a total of 13 arrays are required for 2D cases.

2.2. Viscoelastic model

Both the viscoelastic material and the PML attenuate elastic waves. P-wave and S-wave may have different attenuations in viscoelastic material. In PML, the parameters Ω_x and Ω_z characterize the attenuation of waves propagating along x- and z-direction, respectively, regardless of the type of waves. I modify the NPML formula to attenuate elastic waves like a viscoelastic material. I assume a homogeneous isotropic linear viscoelastic material having the following constitutive relations in the frequency domain

$$\begin{cases} i\omega T_{xx} = \lambda \dfrac{i\omega}{\Omega_\lambda + i\omega}(\partial_x V_x + \partial_z V_z) + 2\mu \dfrac{i\omega}{\Omega_\mu + i\omega}\partial_x V_x \\ i\omega T_{zz} = \lambda \dfrac{i\omega}{\Omega_\lambda + i\omega}(\partial_x V_x + \partial_z V_z) + 2\mu \dfrac{i\omega}{\Omega_\mu + i\omega}\partial_z V_z \\ i\omega T_{xz} = \mu \dfrac{i\omega}{\Omega_\mu + i\omega}(\partial_x V_z + \partial_z V_x) \end{cases}, \tag{11}$$

where Ω_λ and Ω_μ are the dissipation parameters of the viscoelastic material.

Transforming Eq. (2) to the frequency domain gives

$$\begin{cases} i\omega \rho V_x = \partial_x T_{xx} + \partial_z T_{xz} \\ i\omega \rho V_z = \partial_x T_{xz} + \partial_z T_{zz} \end{cases} \tag{12}$$

Equations (11) and (12) constitute the set of the wave equations in the viscoelastic material.

Defining the complex moduli

$$\tilde{\lambda} = \lambda \frac{i\omega}{\Omega_\lambda + i\omega}, \quad \tilde{\mu} = \mu \frac{i\omega}{\Omega_\mu + i\omega}. \tag{13}$$

Equation (13) has the same form as the complex modulus of a Maxwell model given in equation (2.147) by Carcione (2015). The dissipation parameters Ω_λ and Ω_μ are the reciprocals of relaxation times of a Maxwell material. Therefore, the proposed viscoelastic model is equivalent to a Maxwell model.

2.3. Attenuation rate and phase velocity in the viscoelastic model

Using Helmholtz decomposition theorem,

$$\mathbf{u} = \nabla\varphi + \nabla \times \boldsymbol{\psi}, \quad \nabla \cdot \boldsymbol{\psi} = 0. \tag{14}$$

Following the development given by Buchen (1971) and Borcherdt (1973), Eqs. (11) and (12) then lead to

$$\begin{cases} \nabla^2\varphi + k_P^2\varphi = 0 \\ \nabla^2\psi + k_S^2\psi = 0 \end{cases} \tag{15}$$

where φ represents the scalar potential of P-wave, and ψ represents the vector potential of S-wave, and the complex wave numbers are defined by

$$k_P = \omega/\widetilde{v}_P, \quad k_S = \omega/\widetilde{v}_S, \tag{16}$$

and the complex velocities are defined by

$$\widetilde{v}_P = \left(\left(\widetilde{\lambda} + 2\widetilde{\mu}\right)/\rho\right)^{\frac{1}{2}}, \quad \widetilde{v}_s = (\widetilde{\mu}/\rho)^{1/2}. \tag{17}$$

The displacement and particle motion of inhomogeneous plane P-wave and S-wave in viscoelastic medium have been fully discussed by Buchen (1971) and Borcherdt (1973). I am only interested in the attenuation rate and phase velocity in the proposed viscoelastic model. I will begin with S-wave. Let

$$k_P = k_P^R + ik_P^I, \quad k_S = k_S^R + ik_S^I \tag{18}$$

The second parts of Eqs. (13), (16)–(18) lead to

$$k_S^R = \frac{\omega}{v_S^u}\left[\frac{1}{2} + \frac{1}{2}\left(1 + (\Omega_\mu/\omega)^2\right)^{1/2}\right]^{1/2}, \quad k_S^I = -\frac{\Omega_\mu}{2v_S^u}\left[\frac{1}{2} + \frac{1}{2}\left(1 + (\Omega_\mu/\omega)^2\right)^{1/2}\right]^{-1/2} \tag{19}$$

where $v_S^u = (\mu/\rho)^{1/2}$ is the unrelaxed S-wave velocity. Then the phase velocity of S-wave in the viscoelastic material is

$$v_S = \frac{\omega}{k_S^R} = v_S^u\left[\frac{1}{2} + \frac{1}{2}\left(1 + (\Omega_\mu/\omega)^2\right)^{1/2}\right]^{-1/2}. \tag{20}$$

Defining the attenuation rate α of a wave by

$$\alpha = \frac{20}{\Delta x(m)}\log_{10}\left(\frac{\text{Amplitude}(x)}{\text{Amplitude}(x+\Delta x)}\right) \text{ dB/m}. \tag{21}$$

It follows that

$$\alpha_S = -\frac{20}{\ln 10}k_S^I = \frac{4.343\Omega_\mu}{v_S^u}\left[\frac{1}{2} + \frac{1}{2}\left(1 + (\Omega_\mu/\omega)^2\right)^{1/2}\right]^{-1/2} \text{ dB/m}. \tag{22}$$

Both the phase velocity and attenuation rate of S-wave in the viscoelastic material are frequency dependent. If the attenuation rate is normalized by 4.343 Ω_μ/v_s^u, and the phase velocity is normalized by v_s^u, the attenuation rate and phase velocity will be the same function of normalized frequency ω/Ω_μ. Fig. 1 shows the normalized dispersion and attenuation of the viscoelastic model. The curve is the same as that in Fig. 2.4(a) in Carcione (2015) for phase velocity of Maxwell model. The mismatch of Fig. 1 and 2.4(b) in Carcione (2015) will be discussed later. When ω/Ω_μ is greater than 10, the phase velocity and attenuation rate remain constants. In other words, the phase velocity and attenuation rate are frequency independent for ω/Ω_μ>10, then Eq. (22) gives

$$\alpha_S \approx \frac{4.343\Omega_\mu}{v_S^u}. \tag{23}$$

The phase velocity and attenuation of P-wave depend on both Ω_λ and Ω_μ. For $\Omega_\lambda = \Omega_\mu$, Eqs. (20) and (22) can be applied to the P-wave,

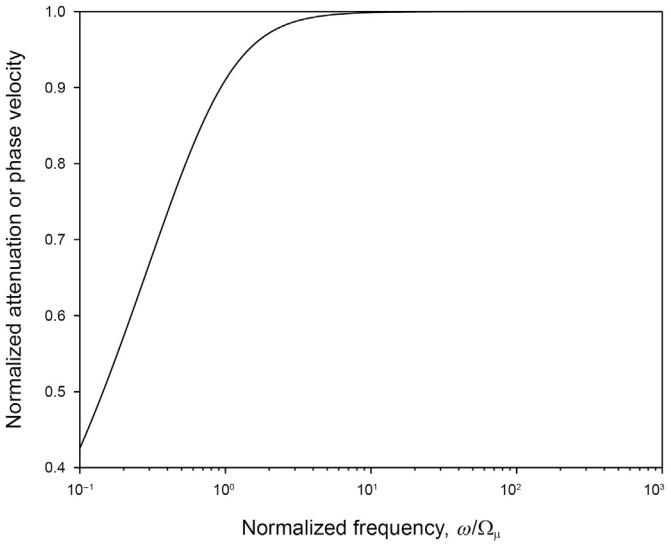

Fig. 1. Dispersion and attenuation of S-wave in the proposed viscoelastic model. The horizontal axis is normalized frequency, and the vertical axis is normalized attenuation rate or phase velocity.

just by replacing the subscript S with P, and where $v_P^u = \sqrt{(\lambda + 2\mu)/\rho}$ is the unrelaxed P-wave velocity. For $\Omega_\lambda \neq \Omega_\mu$, the analytical expressions will be very complicated. However, they can be calculated numerically by combining the first parts of Eqs. (16)–(18), and

$$v_P = \frac{\omega}{k_P^R}, \quad \alpha_P = -\frac{20}{\ln 10}k_P^I. \tag{24}$$

I give some numerical examples in Fig. 2 to show that the phase velocity and attenuation rate for P-wave are very similar to those of S-wave even for $\Omega_\lambda \neq \Omega_\mu$. The density, unrelaxed P-wave velocity and S-wave velocity are 2000 kg/m^3, 4000 m/s, and 2300 m/s, respectively. The horizontal axis is normalized frequency ω/Ω_λ. The phase velocity is normalized by v_P^u, and the attenuation rate is normalized by 4.343 $(\Omega_\lambda+2\Omega_\mu)/3v_P^u$. All the curves coincide as the frequency increasing. A conclusion can be obtained from the Fig. 2,

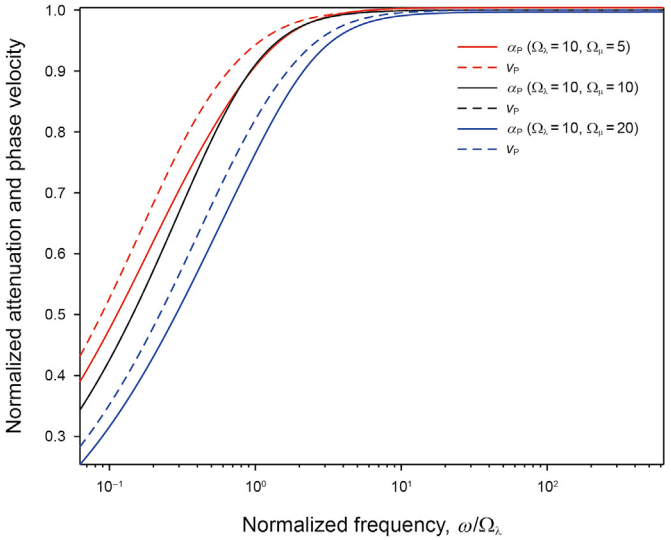

Fig. 2. Dispersion and attenuation of P-wave in the proposed viscoelastic model.

that is, for $\omega/\Omega_\lambda > 10$,

$$\alpha_P \approx \frac{4.343(\Omega_\lambda + 2\Omega_\mu)}{3v_P^u} = \frac{1.448(\Omega_\lambda + 2\Omega_\mu)}{v_P^u}. \tag{25}$$

2.4. Quality factors of the viscoelastic model

Quality factor (Q) is a very common parameter for characterizing wave attenuation in viscoelastic material. I use the definition of quality factor given by Borcherdt (1973), that is, the ratio of the peak energy density stored per cycle of forced oscillation to the loss in energy density during the cycle. Following the development given by Borcherdt (1973) and Carcione et al., (1988b), for homogeneous P-wave and S-wave, I have

$$Q_P = \frac{\mathrm{Re}\left(\widetilde{\lambda} + 2\widetilde{\mu}\right)}{\mathrm{Im}\left(\widetilde{\lambda} + 2\widetilde{\mu}\right)}, \quad Q_S = \frac{\mathrm{Re}(\widetilde{\mu})}{\mathrm{Im}(\widetilde{\mu})}. \tag{26}$$

By introducing an analogous quality factor

$$Q_\lambda = \frac{\mathrm{Re}(\tilde{\lambda})}{\mathrm{Im}(\tilde{\lambda})}, \tag{27}$$

after some derivations, Eqs. (13), (25) and (26) give that

$$Q_\lambda = \frac{\omega}{\Omega_\lambda}, \quad Q_S = \frac{\omega}{\Omega_\mu}, \tag{28}$$

and

$$Q_P = Q_\lambda + \frac{Q_S - Q_\lambda}{1 + \frac{Q_\lambda(1+Q_S^2)}{Q_S(1+Q_\lambda^2)}\frac{\lambda}{2\mu}}. \tag{29}$$

The quality factor of S-wave Q_S is a simple linear function of frequency. Fig. 3 shows the quality factor of P-wave Q_P versus normalized frequency for three cases with various Ω_μ. It is shown that Q_P is also a simple linear function of frequency. The black line ($\Omega_\lambda = \Omega_\mu$) also represents the curve of Q_S versus normalized frequency ω/Ω_μ. The proposed viscoelastic model is not a constant Q model but a linear Q model. Earth materials have been shown to have a nearly constant Q over a specified frequency range (Wuenschel, 1965; Spencer, 1981; Murphy, 1982). The proposed viscoelastic model can be a good approximation of the real material within a given narrow frequency band.

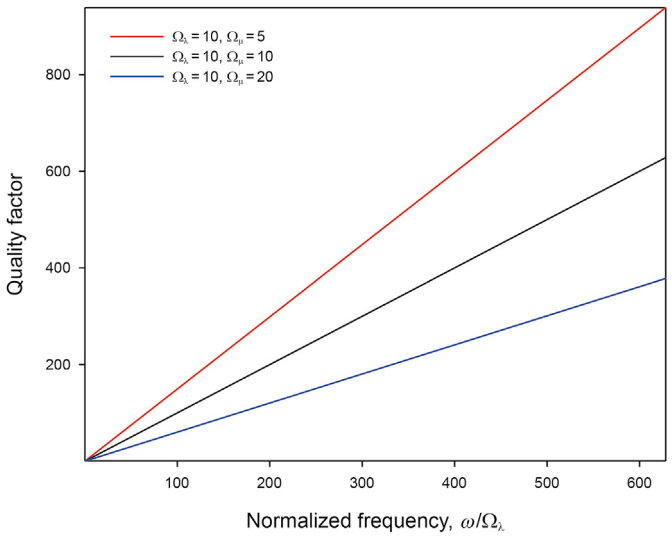

Fig. 3. Quality factor of P-wave in the proposed viscoelastic model.

For a given material with known quality factor, I use the following equations to calculate the dissipation parameters Ω_λ and Ω_μ

$$\Omega_\lambda = \frac{\omega_0}{Q_\lambda}, \quad \Omega_\mu = \frac{\omega_0}{Q_S}, \tag{30}$$

where ω_0 is the central angular frequency of the source in the simulation.

For materials with small absorption, Eq. (26) reduces to (Borcherdt, 1973)

$$Q = -\frac{k^R}{2k^I}. \tag{31}$$

It is the same as the expression obtained by using the definition of Q given by White (1992), that is, the number of wavelengths a wave must travel through the material before its amplitude drops by a factor $e^{-\pi}$. Eqs. (21) and (31) lead to

$$Q = \frac{4.343\omega}{v\alpha}. \tag{32}$$

The subscripts P or S is omitted in Eqs. (31) and (32) since the equations are applicable for both P-wave and S-wave. The dissipation factor of Fig. 2.4(b) in Carcione (2015) is defined to be Q^{-1}. That explains the difference between Fig. 1 and 2.4(b) in Carcione (2015).

2.5. Unified set of equations for viscoelastic model and PML

For incorporating NPML into the viscoelastic wave equations, I use Eq. (3) to stretch the spatial coordinates of Eqs. (11) and (12). Assuming $\Omega_m/\omega < 1$ ($m = P, S, x, z$), and omitting the second order small quantity $\Omega_m\Omega_n/\omega^2$ ($m = P, S$ and $n = x, z$), I have the following sets of wave equations:

$$\begin{cases} i\omega T_{xx} = \lambda\frac{i\omega}{\Omega_\lambda+\Omega_x+i\omega}\partial_x V_x + 2\mu\frac{i\omega}{\Omega_\mu+\Omega_x+i\omega}\partial_x V_x + \lambda\frac{i\omega}{\Omega_\lambda+\Omega_z+i\omega}\partial_z V_z \\ i\omega T_{zz} = \lambda\frac{i\omega}{\Omega_\lambda+\Omega_x+i\omega}\partial_x V_x + \lambda\frac{i\omega}{\Omega_\lambda+\Omega_z+i\omega}\partial_z V_z + 2\mu\frac{i\omega}{\Omega_\mu+\Omega_z+i\omega}\partial_z V_z, \\ i\omega T_{xz} = \mu\frac{i\omega}{\Omega_\mu+\Omega_x+i\omega}\partial_x V_z + \mu\frac{i\omega}{\Omega_\mu+\Omega_z+i\omega}\partial_z V_x \end{cases} \tag{33}$$

$$\begin{cases} i\omega\rho V_x = \frac{i\omega}{\Omega_x+i\omega}\partial_x T_{xx} + \frac{i\omega}{\Omega_z+i\omega}\partial_z T_{xz} \\ i\omega\rho V_z = \frac{i\omega}{\Omega_x+i\omega}\partial_x T_{xz} + \frac{i\omega}{\Omega_z+i\omega}\partial_z T_{zz} \end{cases} \tag{34}$$

where Ω_λ and Ω_μ characterize the attenuation due to viscoelastic absorption, Ω_x and Ω_z characterize the attenuation due to PML. The contribution of viscoelastic absorption and PML absorption can be simply added up. Eqs. (33) and (34) have the same form as Eqs. (5) and (6), the NPML equations for elastic media. Therefore, the NPML technique in subsection 2.1 can be used to process Eqs. (33) and (34).

Wave equations (33) and (34) reduce automatically to the wave equations of interior viscoelastic materials when Ω_x and Ω_z vanish,

and reduce automatically to the wave equations for interior elastic materials when Ω_x, Ω_z, Ω_λ and Ω_μ vanish. Thus, the proposed equations provide a unified basis for elastic media, viscoelastic media and their PML regions.

The approximation in Eqs. (33) and (34), omitting the second order small quantity, only happens when all the Ω_x, Ω_z, Ω_λ and Ω_μ are nonzero, i.e., in the PML region. In the inner region, where $\Omega_x = \Omega_z = 0$, Eqs. (33) and (34) are exact. Since the waves in PML will be attenuated, the error caused by the approximation will not affect the inner region. For simplicity, I refer to the new viscoelastic PML technique as VPML. The FDTD implementation of VPML is the same as NPML. Therefore, the VPML is easier in implementation in existing codes (that without PML and viscoelasticity) than SPML and CPML. All you have to do is adding arrays to store these memory variables and updating them in time loop.

For 2D cases, VPML (including PML regions) requires a total of 15 arrays, which are a little bit more than that required in the NPML method for elastic media (13 arrays). The formulations of 3D geometry are given in the APPENDIX. The VPML technique requires 30 arrays in 3D viscoelastic media. The CPML (Martin and Komatitsch, 2009) and ADE-PML (Martin et al., 2019) requires 39 arrays in 3D viscoelastic media. The memory storage in VPML is about three-fourths of that in CPML and ADE-PML.

Comparing Eq. (9) with Eq. (26) of Komatitsch and Martin (2007), and with Eq. (18) of Martin et al. (2010), one can find that the time-marching formulations for the memory variables in NPML and CPML, and for auxiliary memory variables in ADE-PML, are very similar to each other (note that $\Omega = 1/\tau$).

2.6. Finite difference discretization

The velocity and stress components are discretized to a staggered grid (Virieux, 1986; Levander, 1988) as shown in Fig. 4. According to the elasto-dynamic finite integration technique (Fellinger et al., 1995), the density at the edges, the viscoelastic parameters Ω_λ, Ω_μ, Ω_x and Ω_z at the corners or edges, are set to be the average of corresponding values of the surrounding cells. The shear modulus in the corners are set to be the harmonic mean of shear moduli of the four surrounding cells. The grid has uniform grid spacings Δx and Δz in the x- and z-directions. The spatial derivatives are approximated by forth order central differences, and the temporal derivatives are approximated by second order central differences (Levander, 1988). For the time domain finite difference implementation of Eqs. (33) and (34), the readers are referred to Section 2.1 and Wang and Tang (2003).

3. Examples

3.1. Comparison of the numeric results with the analytic results

First, I verify the VPML method by comparing the numerically simulated waveforms and their spectra with analytical ones. The 2D model is shown in Fig. 5. The model is filled with homogeneous viscoelastic material ($\rho = 1150$ kg/m^3, $v_P = 2260$ m/s, $v_S = 1190$ m/s, $Q_P = 10$, $Q_S = 10$). Note, Q_P and Q_S are the quality factors of P- and S-wave at the central frequency of source, respectively. The ends of z direction are PMLs, and the ends of x direction are set to be periodical boundary conditions. A line velocity source parallel to z axis can vibrate along x direction (z direction), and generate plane P-wave (S-wave) advancing in x-direction. The velocity source is added directly on the right sides of Eq. (34). The source function is

$$g(t) = \left(2\omega_0^2 \Big/ \gamma^2\right) t^2 e^{-\omega_0 t/\gamma} \sin(\omega_0 t) H(t), \tag{35}$$

where $\gamma = 2$ is used to define the band-width of the source spectrum, $\omega_0 = 2\pi f_0$, $f_0 = 10$ kHz the central frequency, and $H(t)$ the Heaviside step function. Four point receivers are equally spaced (1 m) along the x direction. The PMLs are 20 cells thick, and $\beta = 8$. The grid spacings Δx and Δz are both 5.88 mm, the time step Δt is 1.5 μs.

The analytical solutions of plane wave in the unbounded homogeneous viscoelastic material will be

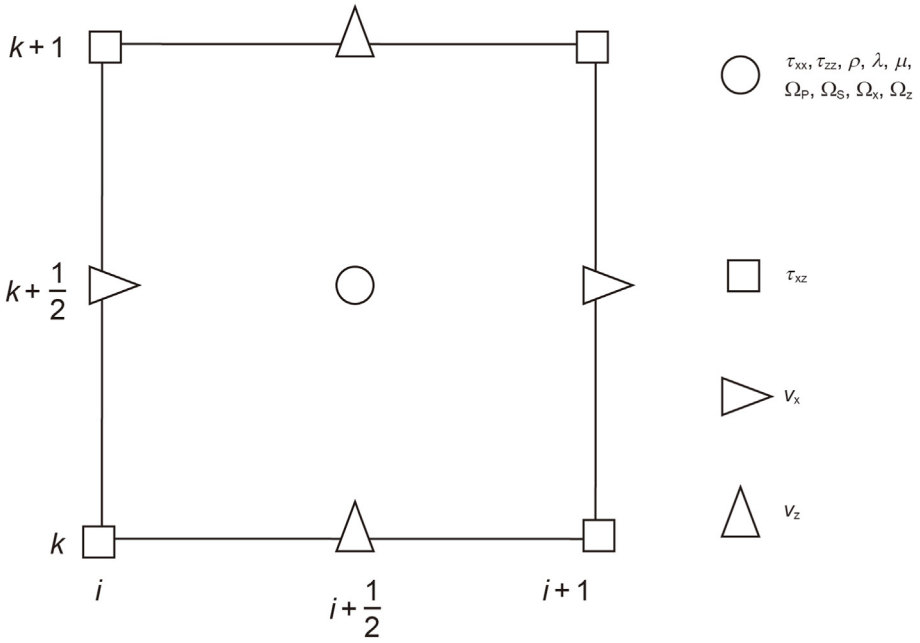

Fig. 4. Elementary cell of staggered grids. Locations where stresses, velocities and viscoelastic parameters are defined.

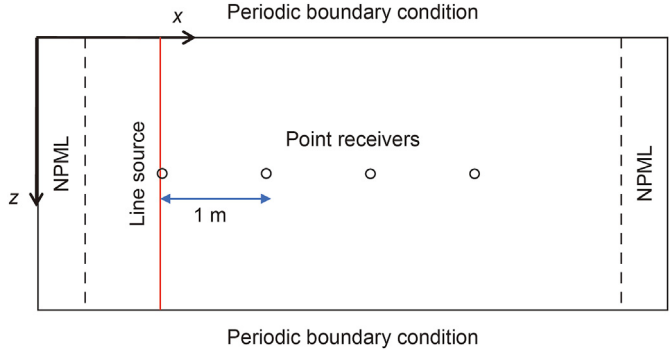

Fig. 5. 2D finite-difference model of plane P-wave and S-wave propagation in unbounded homogeneous viscoelastic material.

$$v_x(x,t) = \frac{1}{2\pi}\int_{-\infty}^{+\infty} G(\omega)e^{i(\omega t - k_P x)}\mathrm{d}\omega, \tag{36}$$

$$v_z(x,t) = \frac{1}{2\pi}\int_{-\infty}^{+\infty} G(\omega)e^{i(\omega t - k_S x)}\mathrm{d}\omega, \tag{37}$$

where, $G(\omega)$ is the Fourier transform of source function $g(t)$, and k_P, k_S are complex wave numbers defined in Eq. (16).

The comparisons of numeric and analytic results are shown in Fig. 6. The agreement of both waveforms and spectra is very good. Only small mismatch present at low frequency. The comparisons for various quality factor are performed. The higher the quality factor, the better the agreement. For $Q > 50$, agreement between numeric and analytic results is perfect. For $Q < 4$, the numerical solution starts to deviate from the analytical solution.

3.2. Attenuation in material with low viscosity

Then, I investigate the attenuation of P-wave and S-wave in unbounded homogeneous viscoelastic solid ($\rho = 1600$ kg/m^3, $v_P = 2800$ m/s, $v_S = 1600$ m/s). The 2D model of this example is shown in Fig. 7. The left top corner of the interior region is defined as the origin of coordinate system. The interior region (the dashed rectangle, 20 cm by 10 cm) is surrounded by PMLs. The PMLs are 15 cells thick, and $\beta = 10$. The grid spacings Δx and Δz are both 0.5 mm, ensuring that at least 13 cells per wavelength are used. The time step Δt is 0.1 μs. A point force source vibrating along a direction of 45° to the x-direction, is located at (5,5) cm. The source signal is

$$g(t) = (1+\cos(2\pi(t-t_c/2)/t_c))\cos(\omega_0(t-t_c/2))(H(t)-H(t-t_c)), \tag{38}$$

where $\omega_0 = 2\pi f_0$, $f_0 = 250$ kHz the central frequency. $t_c = 3/f_0$ the duration of source impulse. Both P-wave and S-wave can be excited simultaneously in the material. There are two point receivers with 5 cm spacing. The near one R1 is 10 cm from the source. The x- and z-component of particle velocity are recorded by the receivers.

First, the model is filled with purely elastic solid, $Q_P = \infty$ and $Q_S = \infty$, that is $\Omega_\lambda = 0$, and $\Omega_\mu = 0$. Fig. 8 shows the simulated waveforms, their Fourier amplitude spectra, and attenuation in frequency domain. P-wave is dominant in the waveforms of v_x component. A 20 μs-width rectangular window is applied to the waveform of v_x to exclude S-wave. The Fourier transformation of the signal in the rectangular window gives the Fourier amplitude spectra of P-wave. The attenuation in frequency domain is computed by comparing the Fourier amplitude spectra of the near and far receivers using Eq. (21). This method is also used for S-wave extraction from v_z component.

There is no material attenuation in elastic material. The attenuation is caused by geometric spread. The geometric spreading of wave excited by a point source in 2D plane is proportional to the reciprocal of the square root of the distance from the source. The amplitude ratio of R1 and R2 is $(3/2)^{1/2}$. Using Eq. (21), the theoretical geometric spread attenuation from R1 to R2 will be 0.3522 dB/cm. Fig. 6 gives that the numerical geometric spread attenuation of P-wave and S-wave are 0.3536 dB/cm and 0.3543 dB/cm, respectively. The error between numerical values and the

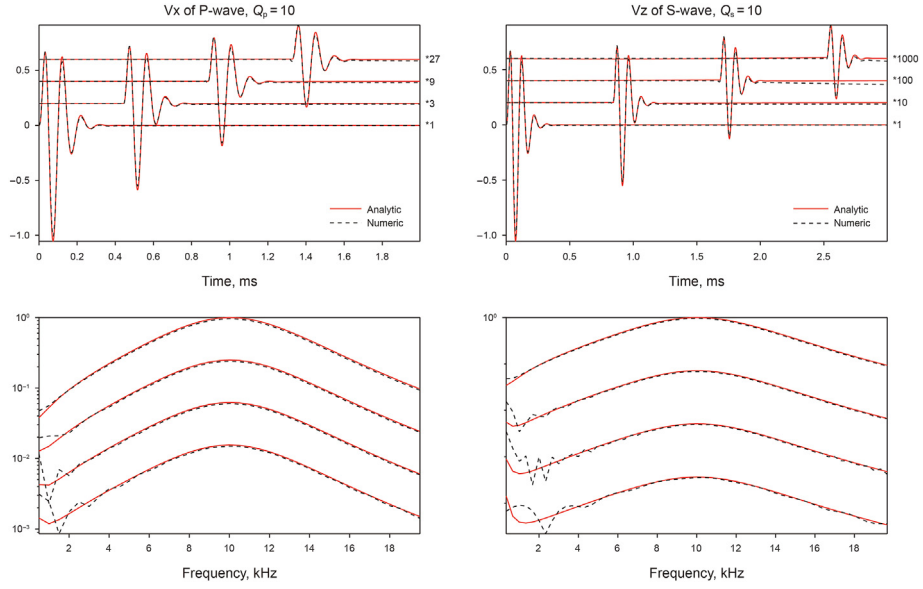

Fig. 6. The comparison of numerical and analytic waveforms and their spectra for plane P-wave and S-wave propagating in unbounded homogeneous elastic solid with $Q_P = 10$, $Q_S = 10$. Left panel: particle velocity v_x, for plane P-wave. Right panel: particle velocity v_z for plane S-wave. The numbers listed on the left side of waveform are the multiples that the waveform is amplified.

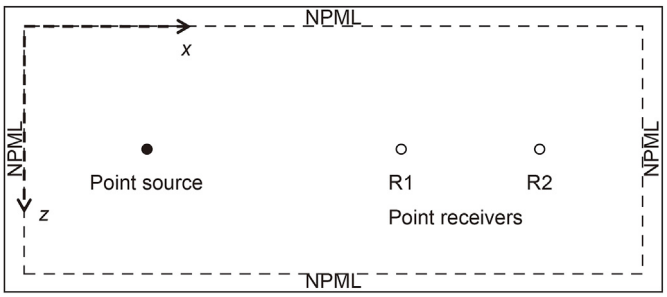

Fig. 7. 2D finite-difference model of wave propagation in unbounded homogeneous viscoelastic material.

theoretical values are negligible.

Then, the model is filled with viscoelastic solid with $Q_\lambda = 40$, $Q_S = 30$. Equation (29) gives that $Q_P = 32.85$. Note that the proposed viscoelastic model is not a constant Q model. Q_λ and Q_S are used to calculate Ω_λ and Ω_μ by Eq. (30). Then the default material attenuations can be obtained using Eqs. (23) and (25), which are $\alpha_P = 0.7446$ dB/cm, and $\alpha_S = 1.421$ dB/cm. The waveforms, amplitude spectra and attenuation are shown in Fig. 9. The total attenuation is caused by geometric spreading and viscoelastic absorption.Figs. 8 and 9 have the same model geometry. It follows that the geometric spreading attenuation will be the same value. Deducting the geometric spreading attenuation (0.3536 dB/cm) from the total attenuation (1.0931 dB/cm), gives the numerical material attenuation of P-wave 0.7395 dB/cm, which has a negligible error (0.7%) from the default material attenuation of P-wave. Similar analysis gives the numerical material attenuation of S-wave is 1.4187 dB/cm, which has a very small deviation (0.16%) from the default value 1.421 dB/cm.

Above numerical examples demonstrate that P-wave and S-wave in the proposed viscoelastic model have constant attenuation for in low attenuative material. The material attenuation can be exactly defined by quality factors of P-wave and S-wave.

3.3. Attenuation in material with high viscosity

Most of the known viscoelastic models in finite difference techniques are designed to treat materials with low absorption, but fail to produce accurate or even physically meaningful results for highly attenuative materials (Asvadurov et al., 2003). I will demonstrate that the proposed viscoelastic model works well for highly attenuative materials.

The model is the same as that shown in Fig. 7. However, the point force source is located at (3,5) cm. There are seven point receivers in straight line along x-direction with 1 cm spacing. The nearest one R1 is 1 cm from the source. The model is filled with highly attenuative solid ($Q_P = 3.294$, $Q_\lambda = 4$, $Q_S = 3$). Since $Q_P < 10$ and $Q_S < 10$, the attenuation rate of P-wave and S-wave are not constants but frequency dependent functions. The theoretical attenuation rate of S-wave can be obtained directly from Eq. (22). The theoretical attenuation rate of P-wave can be calculated numerically by using Eq. (24). Fig. 10 shows the waveforms of x- and z-component of particle velocity recorded by receivers R6 and R7, their amplitude spectra, numerical and theoretical attenuation rate. In Fig. 10(b), both P-wave and S-wave appear in z-component of particle velocity. The P-wave is excluded by a 20 μs-width rectangular window to obtain the attenuation of S-wave. The geometric spreading attenuation is deducted from the total attenuation. The numerical material attenuations of both P-wave and S-wave have a good agreement with the theoretical material attenuation in the effective frequency band of the source.

One interesting phenomenon in Fig. 10(b) is that P-wave appears at a very strong amplitude in the particle-velocity component perpendicular to the direction of wave propagation, that is very

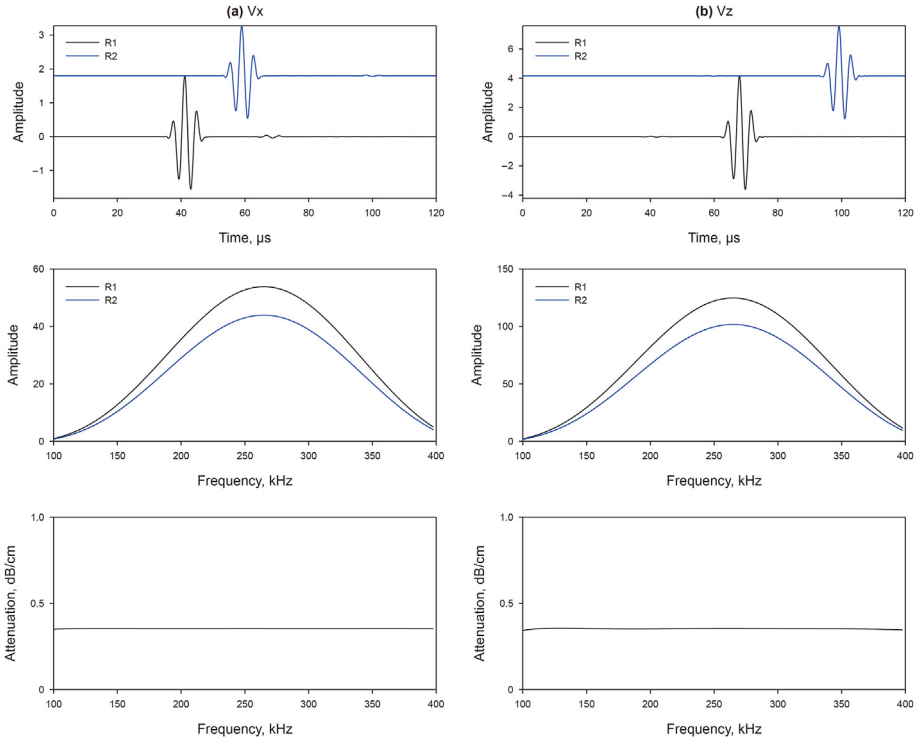

Fig. 8. The simulated waveforms of particle velocity, Fourier amplitude spectra and attenuation in frequency domain, in unbounded homogeneous elastic solid with $Q_P = \infty$, $Q_S = \infty$. (a) x-component of particle velocity v_x, and (b) z-component of particle velocity v_z.

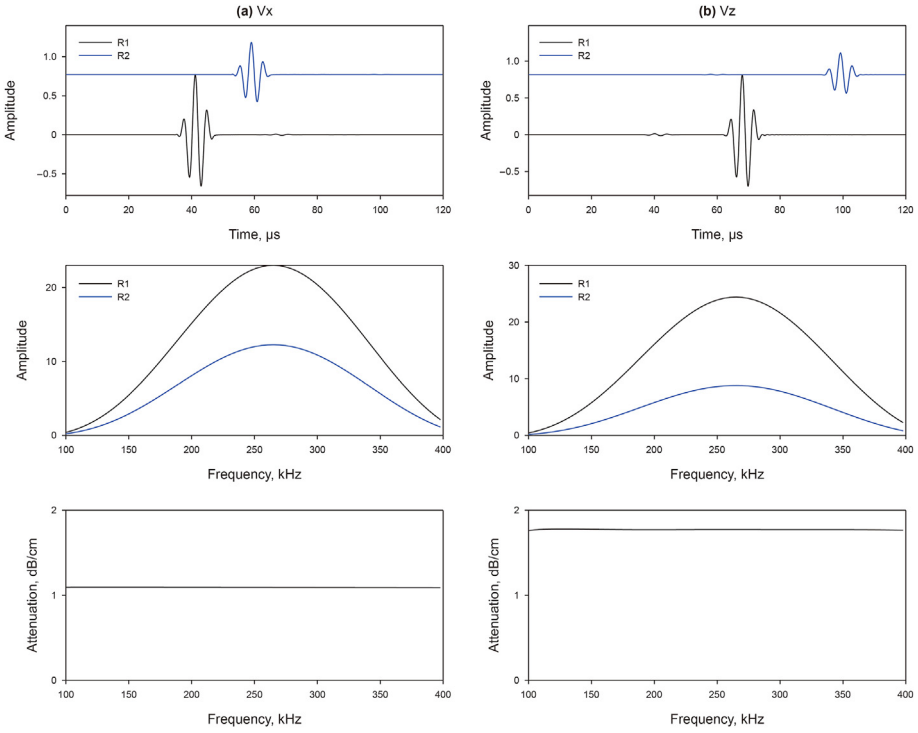

Fig. 9. Same as Fig. 8 except for $Q_P = 32.85$, $Q_S = 30$.

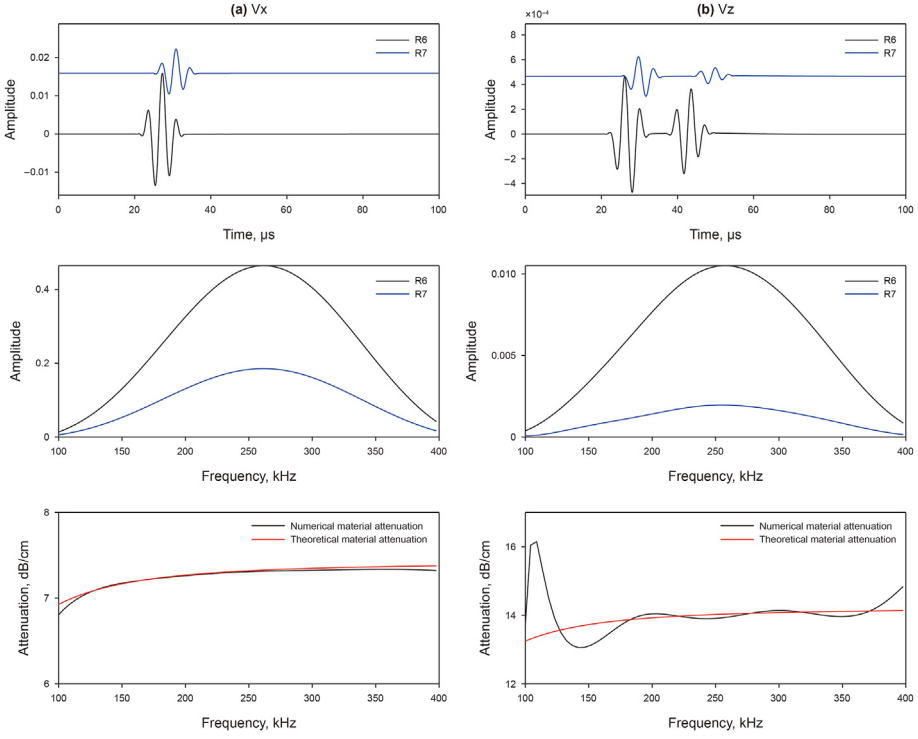

Fig. 10. Same as Fig. 8 except for $Q_P = 3.294$, $Q_S = 3$. The geometric spread attenuation has been deducted from the total attenuation.

different from the waveform in purely elastic material shown in Fig. 8(b). It is because that, in a viscoelastic material, the inhomogeneous P-wave or S-wave have elliptical particle motion, and the direction of maximum energy flow is not the direction of phase propagation (Buchen, 1971; Borcherdt, 1973).

Next, the model is filled with solid of very high viscosity ($Q_\lambda = 1.2$, $Q_S = 1$, and hence $Q_P = 1.07$). The simulated waveforms are shown in Fig. 11. PMLs are unnecessary because the waves disappear before they strike the model boundaries. The waves attenuate so rapidly that the waveforms recorded by the far

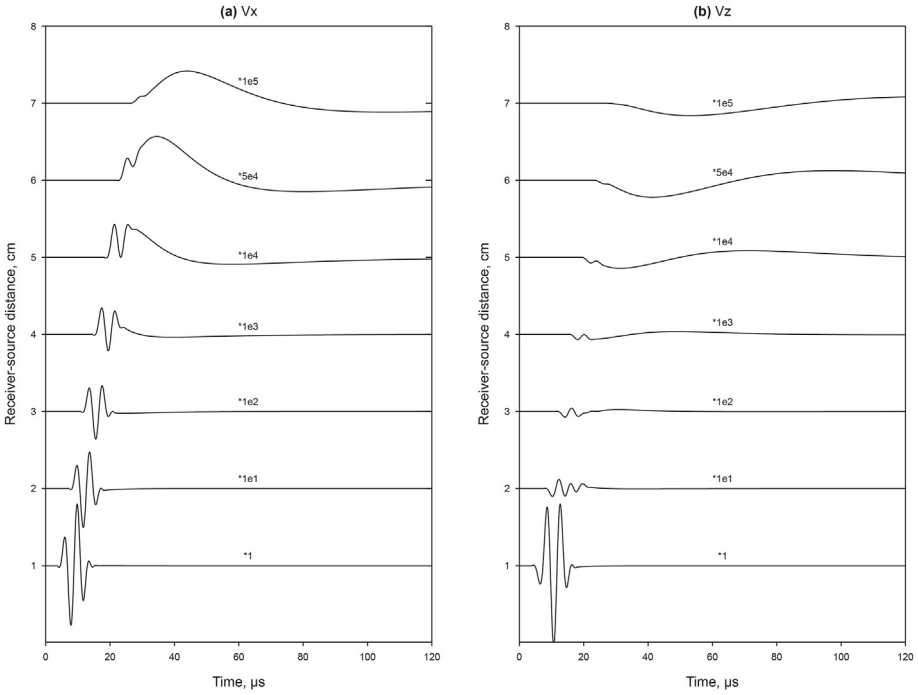

Fig. 11. The simulated waveforms of particle velocity in homogeneous viscoelastic solid with $Q_P = 1.07$, $Q_S = 1$. (a) x-component of particle velocity, and (b) z-component of particle velocity. The number listed above each waveform is the multiple that the waveform is amplified.

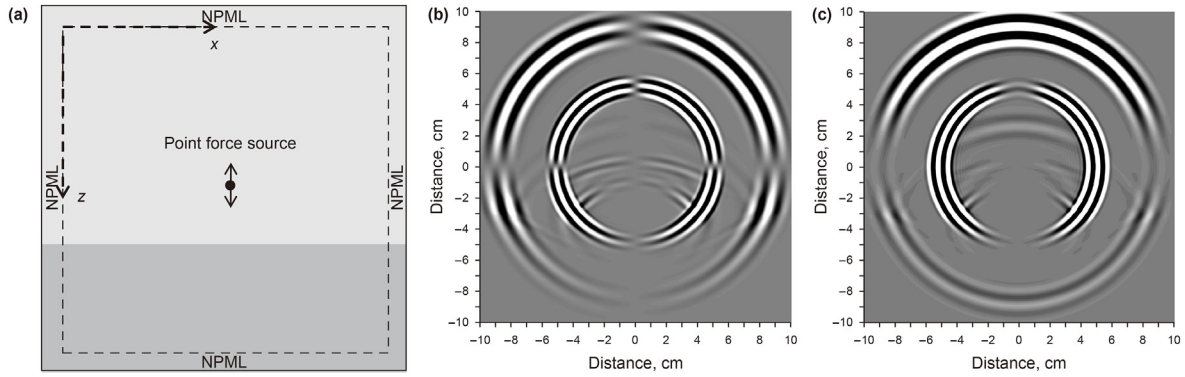

Fig. 12. Reflections at the interface of two viscoelastic material with different viscosity. (a) Finite-difference model. The quality factors are $Q_P = 43$, $Q_S = 40$ for upper layer, and $Q_P = 4.3$, $Q_S = 4$ for the lower layer. (b) Snapshot of x-component of particle velocity at 40 μs. (c) Snapshot of z-component of particle velocity at 40 μs.

receivers have to be amplified in order to be plotted in one panel. The numbers listed in Fig. 11 are how many times the amplitude has been amplified. There are no longer distinct wave packets of P-wave and S-wave. Only low frequency components of the original wave packet survive after propagating 6 cm (from R1 to R7). Their amplitudes drop to several millionths. The computation is stable for highly attenuative material.

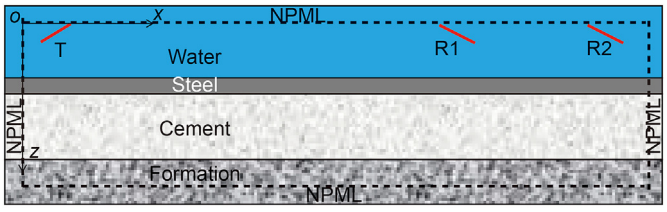

Fig. 13. Finite-difference model of leaky Lamb wave in layered viscoelastic materials.

3.4. Reflection due to inhomogeneity of viscosity

Example shown in Fig. 12 illustrates the reflection due to inhomogeneity of viscosity. The interior region of the model is a 20 cm by 20 cm square, which is divided into two layers. The upper layer has quality factors $Q_\lambda = 50$ ($Q_P = 43$), $Q_S = 40$, and the lower layer has quality factors $Q_\lambda = 5$ ($Q_P = 4.3$), $Q_S = 4$. Both layers have the same density, P- and S-wave velocities. A point force source vibrating along z-direction is located at the center of the square (10,10) cm. The interface is located at $z = 14$ cm. Fig. 12 (b) and (c) are the snapshots of v_x and v_z component at 40μs. There are reflected P-wave and S-wave while P-wave or S-wave strikes on the interface. The v_x component is antisymmetric across the interface at $z = 14$ cm, and the v_z component is symmetric across the interface. More examples show that the reflection coefficient is proportional to the viscosity contrasts between the two layers. This phenomenon is caused by the reflection of inhomogeneous waves and is consistent with the prediction by Borcherdt (1982). Therefore, the

Table 1
Acoustic parameters of finite difference model.

Layer	Thickness, cm	ρ, kg/m^3	v_P, m/s	v_S, m/s	Q_λ	Q_S	Q_P
Water	3.2	1000	1500	–	100	–	100
Steel	0.8	7800	5930	3250	1000	1000	1000
Cement	4	1150	2260	1190	18	15	15.9
Formation	2	2180	3960	2350	30	25	26.5

parameters in PML regions have to be gradual to minimize the reflection due to inhomogeneous viscosity.

3.5. Leaky lamb wave in multi-layered structure

In this example, leaky Lamb waves in layered viscoelastic materials are simulated. The background is about the cement bond evaluation (Al-Suwaidi et al., 2009). The model is shown in Fig. 13. It is a 4-layered model used to approximate a cased well filled with cement between the steel casing and the formation. The transmitter is simulated by point sources arranged in a 2 cm line. To generate and receive Lamb wave, the inclination angle of transmitter and receiver is 36°. The coordinates of the transmitter center are (3 cm, 1 cm). There are two line-receivers, 10 cm apart. The distance between the transmitter and the first receiver R1 is 30 cm. The recorded waveform is the mean value across the line-receiver. The material parameters are listed in Table 1. Fig. 14 shows the simulated waveforms and snapshots of stress component τ_{xx}. For comparison, Fig. 15 shows the same results for purely elastic materials, which are obtained just by setting the viscoelastic parameters Ω_λ and Ω_μ of all layers to be zero. The first arrival is zero-order symmetric mode (S0) of Lamb wave in the steel plate, which is suppressed by the special tilt angle of transmitter and receivers. The second arrival is zero-order anti-symmetric mode (A0) of Lamb wave, which is also called as the leaky

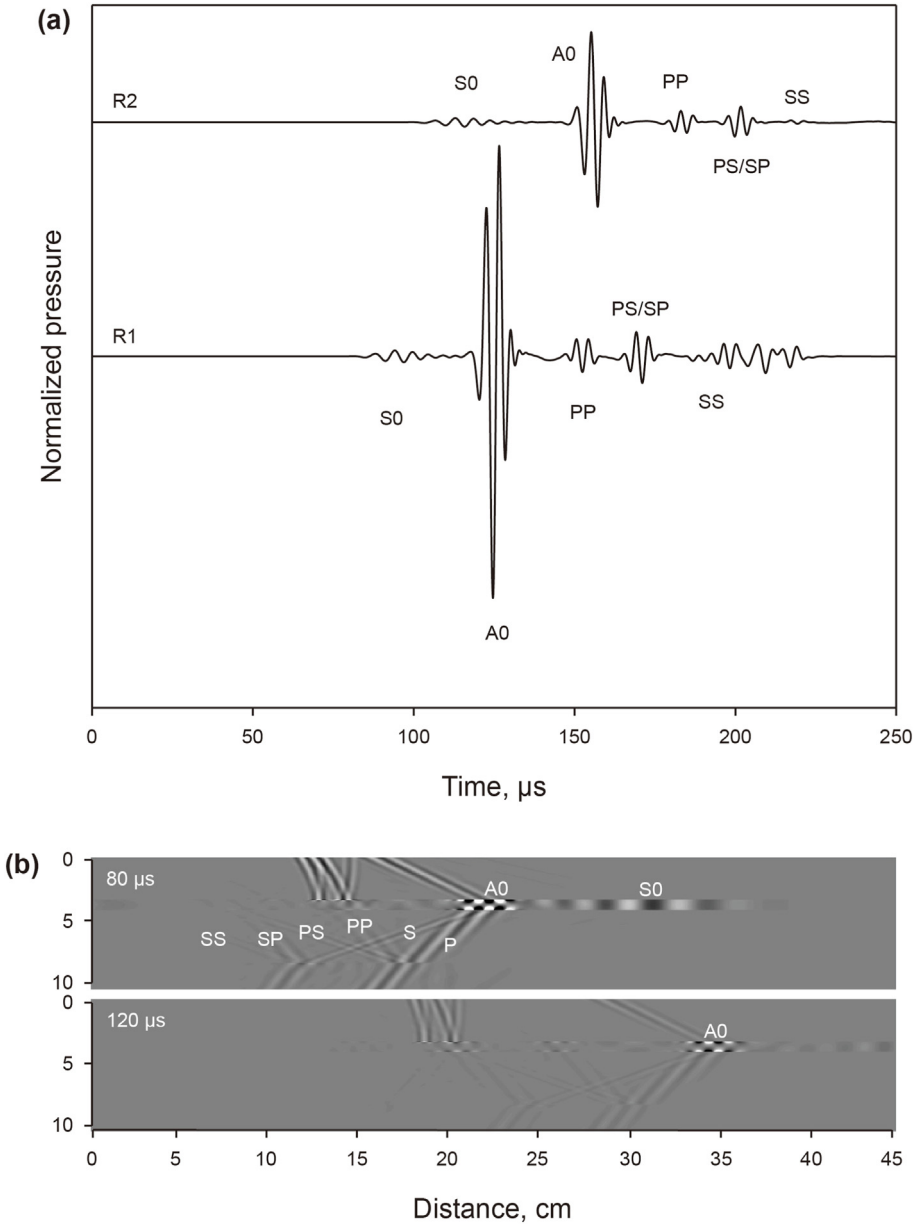

Fig. 14. The simulated waveforms (a) and snapshots of stress component τ_{xx} (b) of the model shown in Fig. 13. The model parameters are shown in Table 1.

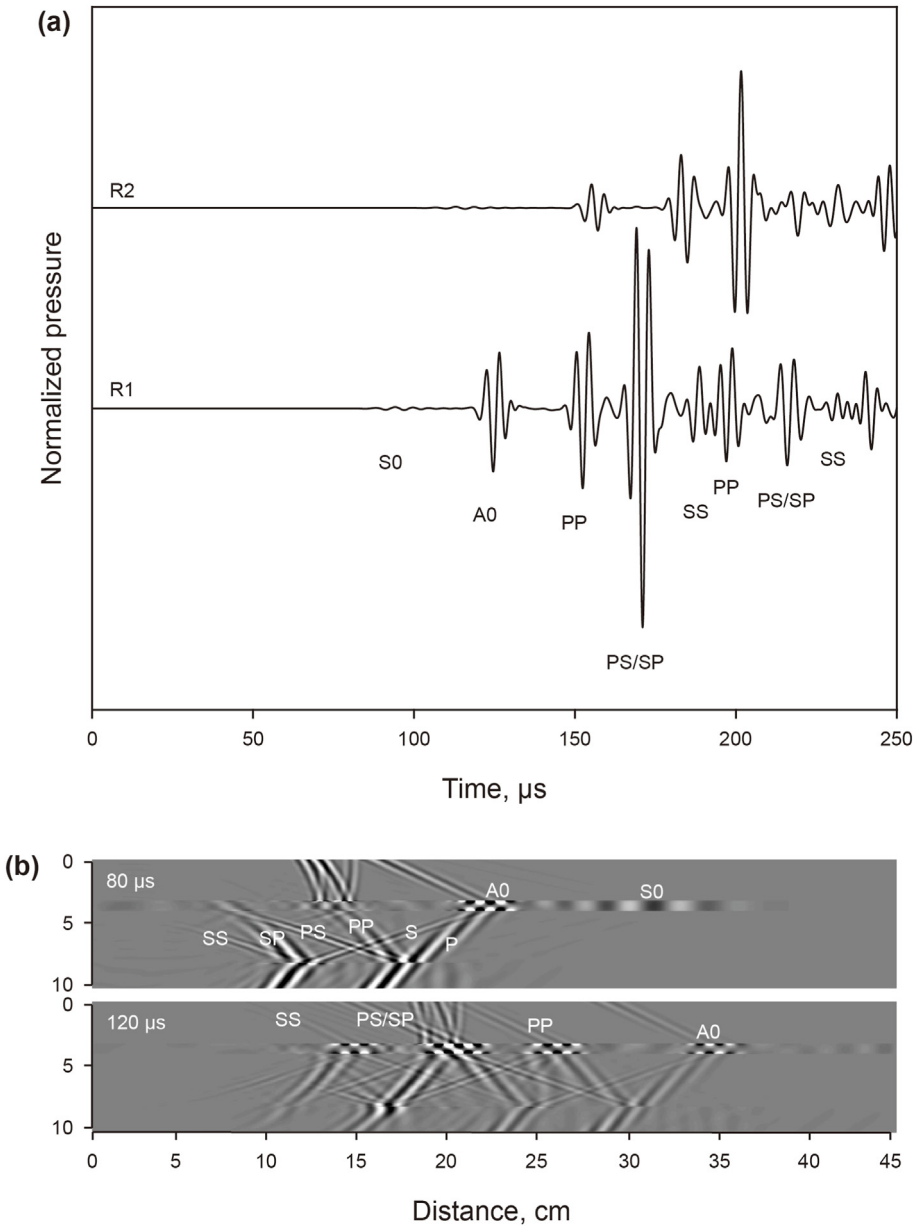

Fig. 15. Same as Fig. 14 except for that all the materials are purely elastic.

Lamb wave, or flexural wave. The flexural wave radiates into the cement in the form of P-wave and S-wave, which can be reflected by the third interface (cement-formation interface). These reflections (PP, PS/SP, SS), also known as the third interface echo (TIE). The time difference between TIEs and primary A0 depends on the thickness and wave velocity of cement annulus. Therefore, TIEs can be used to image cement annulus geometry (Al-Suwaidi et al., 2009). The amplitude of TIEs depends on the cement viscosity and the roughness of third interface. Light cement usually has high absorption. The use of light cement in well completion will bring additional difficulty to the geometric imaging of cement annulus.

4. Conclusions

By modifying the NPML formula, I develop the VPML method to simulate the wave propagation in viscoelastic materials and their PMLs. The VPML method, which provides a unified basis for elastic media, viscoelastic media, and their PML regions, is easier in implementation in existing FDTD codes than existing PML techniques. The memory storage required in VPML is about three-fourths of that required in CPML. Another advantage of VPML method is that it is stable in simulating waves in highly attenuative materials ($Q = 1$).

The proposed viscoelastic model is equivalent to Maxwell model. The relations between dissipation parameters Ω_λ, Ω_μ and quality factors Q_P and Q_S are established. For viscosity material with $Q > 10$, which covers most of the real material, the viscoelastic model has frequency independent attenuation and phase velocities. For material of high viscosity ($Q < 10$), both the attenuation and phase velocities depend on frequency. Numerical examples show that the dissipation parameters can accurately characterize

the attenuation of P-wave and S-wave. The contrasts in viscosity at boundaries give rise to reflected waves. The example about leaky Lamb waves in multi-layered structure demonstrates that the VPML method is also stable for heterogeneous media with high acoustic impedance contrast and viscosity contrast.

Declaration of competing interest

The authors declare that they have no known competing financial interests or personal relationships that could have appeared to influence the work reported in this paper.

Appendix. Formulations for 3D cases

The set of wave equations of VPML method for 3D cases can be easily extended from the formulations for 2D casing.

$$\begin{cases} i\omega T_{xx} = \lambda \dfrac{i\omega}{\Omega_\lambda + \Omega_x + i\omega}\partial_x V_x + \lambda \dfrac{i\omega}{\Omega_\lambda + \Omega_y + i\omega}\partial_y V_y + \lambda \dfrac{i\omega}{\Omega_\lambda + \Omega_z + i\omega}\partial_z V_z + 2\mu \dfrac{i\omega}{\Omega_\mu + \Omega_x + i\omega}\partial_x V_x \\ i\omega T_{yy} = \lambda \dfrac{i\omega}{\Omega_\lambda + \Omega_x + i\omega}\partial_x V_x + \lambda \dfrac{i\omega}{\Omega_\lambda + \Omega_y + i\omega}\partial_y V_y + \lambda \dfrac{i\omega}{\Omega_\lambda + \Omega_z + i\omega}\partial_z V_z + 2\mu \dfrac{i\omega}{\Omega_\mu + \Omega_y + i\omega}\partial_y V_y \\ i\omega T_{zz} = \lambda \dfrac{i\omega}{\Omega_\lambda + \Omega_z + i\omega}\partial_x V_x + \lambda \dfrac{i\omega}{\Omega_\lambda + \Omega_y + i\omega}\partial_y V_y + \lambda \dfrac{i\omega}{\Omega_\lambda + \Omega_x + i\omega}\partial_z V_z + 2\mu \dfrac{i\omega}{\Omega_\mu + \Omega_z + i\omega}\partial_z V_z \\ i\omega T_{xy} = \mu \dfrac{i\omega}{\Omega_\mu + \Omega_x + i\omega}\partial_x V_y + \mu \dfrac{i\omega}{\Omega_\mu + \Omega_y + i\omega}\partial_y V_x \\ i\omega T_{xz} = \mu \dfrac{i\omega}{\Omega_\mu + \Omega_x + i\omega}\partial_x V_z + \mu \dfrac{i\omega}{\Omega_\mu + \Omega_z + i\omega}\partial_z V_x \\ i\omega T_{yz} = \mu \dfrac{i\omega}{\Omega_\mu + \Omega_y + i\omega}\partial_y V_z + \mu \dfrac{i\omega}{\Omega_\mu + \Omega_z + i\omega}\partial_z V_y \end{cases} . \tag{A1}$$

$$\begin{cases} i\omega\rho V_x = \dfrac{i\omega}{\Omega_x + i\omega}\partial_x T_{xx} + \dfrac{i\omega}{\Omega_y + i\omega}\partial_y T_{xy} + \dfrac{i\omega}{\Omega_z + i\omega}\partial_z T_{xz} \\ i\omega\rho V_y = \dfrac{i\omega}{\Omega_x + i\omega}\partial_x T_{xy} + \dfrac{i\omega}{\Omega_y + i\omega}\partial_y T_{yy} + \dfrac{i\omega}{\Omega_z + i\omega}\partial_z T_{yz} \\ i\omega\rho V_z = \dfrac{i\omega}{\Omega_x + i\omega}\partial_x T_{xz} + \dfrac{i\omega}{\Omega_y + i\omega}\partial_y T_{yz} + \dfrac{i\omega}{\Omega_z + i\omega}\partial_z T_{zz} \end{cases} . \tag{A2}$$

where V_x, V_y, V_z, T_{xx}, T_{yy}, T_{zz}, T_{xy}, T_{xz} and T_{yz} are the velocity and stress fields in the frequency domain. Ω_λ and Ω_μ characterize the attenuation due to viscoelastic absorption. Ω_x, Ω_y and Ω_z characterize the attenuation due to PML absorption. A total of 30 variables are required. Nine of them are the velocity and stress fields, and 21 of them are memory variables.

References

Al-Suwaidi, A.S., Al-Marri, F., Sultan, E., Jammeli, K., Al-Kindi, Z., Elkadi, A., 2009. Increased certainty in the determination of zonal isolation through the integration of annulus geometry imaging and improved solid-fluid discrimination. In: The 16th SPE Middle East Oil & Gas Show and Conference, pp. 513–521.

Asvadurov, S., Knizhnerman, L., Pabon, J., 2003. Finite-difference modeling of viscoelastic materials with quality factors of arbitrary magnitude. Geophysics 69 (3), 817–824. https://doi.org/10.1190/1.1759468.

Bérenger, J.P., 1994. A perfectly matched layer for the absorption of electromagnetic waves. J. Comput. Phys. 114, 185–200. https://doi.org/10.1006/jcph.1994.1159.

Bérenger, J.P., 1997. Improved PML for the FDTD solution of wave structure interaction problems. IEEE Trans. Antenn. Propag. 45, 466–473. https://doi.org/10.1109/8.558661.

Bérenger, J.P., 1998. An effective PML for the absorption of evanescent waves in waveguides. IEEE Microw. Guid. Wave Lett. 8, 188–190. https://doi.org/10.1109/75.668706.

Bérenger, J.P., 1999. Evanescent waves in PML's: origin of the numerical reflection in wave-structure interaction problems. IEEE Trans. Antenn. Propag. 47, 1497–1503. https://doi.org/10.1109/8.805891.

Bérenger, J.P., 2002a. Application of the CFS PML to the absorption of evanescent waves in waveguides. IEEE Microw. Wireless Compon. Lett. 12, 218–220. https://doi.org/10.1109/LMWC.2002.1010000.

Bérenger, J.P., 2002b. Numerical reflection from FDTD-PMLs: a comparison of the Split PML with the unsplit and CFS PMLs. IEEE Trans. Antenn. Propag. 50, 258–265. https://doi.org/10.1109/8.999615.

Blanch, J.O., Robertsson, J.O., Symes, W.W., 1995. Modeling of a constant Q: methodology and algorithm for an efficient and optimally inexpensive viscoelastic technique. Geophysics 60, 176–184. https://doi.org/10.1190/1.1443744.

Borcherdt, R.D., 1973. Energy and plane waves in linear viscoelastic media. J. Geophys. Res. 78, 2442–2453. https://doi.org/10.1029/JB078i014p02442.

Borcherdt, R.D., 1982. Reflection-refraction of general P- and type-I S-waves in elastic and anelastic solids. Geophys. J. Roy. Astron. Soc. 70, 621–638. https://doi.org/10.1111/j.1365-246X.1982.tb05976.x.

Buchen, P.W., 1971. Plane waves in linear viscoelastic media. Geophys. J. Roy. Astron. Soc. 23, 531–542. https://doi.org/10.1111/j.1365-246X.1971.tb01841.x.

Carcione, J.M., 2009. Theory and modeling of constant-Q P- and S-waves using fractional time derivatives. Geophysics 74. https://doi.org/10.1190/1.3008548. T1–T11.

Carcione, J.M., 2015. Wave Fields in Real Media. Theory and Numerical Simulation of Wave Propagation in Anisotropic, Anelastic, Porous and Electromagnetic Media, third ed. Elsevier Science, pp. 63–122.

Carcione, J.M., Kosloff, D., 2013. Representation of matched-layer kernels with viscoelastic mechanical models. Int. J. Numer. Anal. Model. 10, 221–232.

Carcione, J.M., Kosloff, D., Kosloff, R., 1988a. Wave propagation simulation in a linear viscoacoustic medium. Geophys. J. Roy. Astron. Soc. 93, 393–401. https://doi.org/10.1111/j.1365-246X.1988.tb02010.x.

Carcione, J.M., Kosloff, D., Kosloff, R., 1988b. Wave propagation simulation in a linear viscoelastic medium. Geophys. J. Roy. Astron. Soc. 95, 597–611. https://doi.org/10.1111/j.1365-246X.1988.tb06706.x.

Carcione, J.M., Cavallini, F., Mainardi, F., Hanyga, A., 2002. Time-domain modeling of constant-Q seismic waves using fractional derivatives. Pure Appl. Geophys. 159, 1719–1736. https://link.springer.com/article/10.1007/s00024-002-8705-z.

Chew, W.C., Liu, Q.H., 1996. Perfectly matched layers for elastodynamics: a new absorbing boundary condition. J. Comput. Acoust. 4, 341–359. https://doi.org/10.1142/S0218396X96000118.

Chew, W.C., Weedon, W.H., 1994. A 3D perfectly matched medium from modified Maxwell's equations with stretched coordinates. Microw. Opt. Technol. Lett. 7, 599–604. https://doi.org/10.1002/mop.4650071304.

Collino, F., Tsogka, C., 2001. Application of the perfectly matched absorbing layer model to the linear elastodynamic problem in anisotropic heterogeneous media. Geophysics 66, 294–307. https://doi.org/10.1190/1.1444908.
Day, S.M., Minster, J.B., 1984. Numerical simulation of attenuated wavefields using a Pade approximant method. Geophys. J. Int. 78, 105–118. https://doi.org/10.1111/j.1365-246X.1984.tb06474.x.
Dhemaied, A., Rejiba, F., Camerlynck, C., Bodet, L., Guérin, R., 2011. Seismic-wave propagation modeling in viscoelastic media using the auxiliary differential equation method. Bull. Seismol. Soc. Am. 101 (6), 413–420. https://doi.org/10.1785/0120100064.
Drossaert, F.H., Giannopoulos, A., 2007. A nonsplit complex frequency shifted PML based on recursive integration for FDTD modeling of elastic waves. Geophysics T9–T17 72. https://doi.org/10.1190/1.2424888.
Emmerich, H., Korn, M., 1987. Incorporation of attenuation into time domain computations of seismic wave fields. Geophysics 52, 1252–1264. https://doi.org/10.1190/1.1442386.
Fabien-Ouellet, G., Gloaguen, E., Giroux, B., 2017. Time-domain seismic modeling in viscoelastic media for full waveform inversion on heterogeneous computing platforms with Open CL. Comput. Geosci. 100, 142–155. https://doi.org/10.1016/j.cageo.2016.12.004.
Fan, N., Zhao, L.F., Xie, X.B., Ge, Z.X., Yao, Z.X., 2016. Two-dimensional time-domain finite-difference modeling for viscoelastic seismic wave propagation. Geophys. J. Int. 206, 1539–1551.
Fellinger, P., Marklein, R., Langenberg, K.J., Klaholz, S., 1995. Numerical modelling of elastic wave propagation and scattering with EFIT elastodynamic finite integration technique. Wave Motion 21, 47–66. https://doi.org/10.1016/0165-2125(94)00040-C.
Kelvin, L., Thomson, W., 1875. Mathematical and Physical Papers, vol. 3. Cambridge University Press, Cambridge, p. 27.
Kjartansson, E., 1979. Constant Q-wave propagation and attenuation. J. Geophys. Res. 84, 4737–4748.
Komatitsch, D., Martin, R., 2007. An unsplit convolutional perfectly matched layer improved at grazing incidence for the seismic wave equation. Geophysics 72, SM155–SM167. https://doi.org/10.1190/1.2757586.
Kuzuoglu, M., Mittra, R., 1996. Frequency dependence of the constitutive parameters of causal perfectly matched anisotropic absorbers. IEEE Microw. Guid. Wave Lett. 6, 447–449. https://doi.org/10.1109/75.544545.
Levander, A.R., 1988. Fourth-order finite-difference P-SV seismograms. Geophysics 53, 1425–1436. https://doi.org/10.1190/1.1442422.
Liu, Q.H., Sinha, B.K., 2003. A 3D cylindrical PML/FDTD method for elastic waves in fluid-filled pressurized boreholes in triaxially stressed formations. Geophysics 68, 1731–1743. https://doi.org/10.1190/1.1620646.
Liu, Q.H., Tao, J., 1997. The perfectly matched layer for acoustic waves in absorptive media. J. Acoust. Soc. Am. 102, 2072–2082. https://doi.org/10.1121/1.419657.
Liu, H.P., Anderson, D.L., Kanamori, H., 1976. Velocity dispersion due to anelasticity: implications for seismology and mantle composition. Geophys. J. Roy. Astron. Soc. 47, 41–58. https://doi.org/10.1111/j.1365-246X.1976.tb01261.x.
Liu, X.B., Chen, J.Y., Zhao, Z.C., Lan, H.Q., Liu, F.P., 2018. Simulating seismic wave propagation in viscoelastic media with an irregular free surface. Pure Appl. Geophys. 2018 (2), 1–21.
Martin, R., Komatitsch, D., 2009. An unsplit convolutional perfectly matched layer technique improved at grazing incidence for the viscoelastic wave equation. Geophys. J. Int. 179, 333–344.
Martin, R., Komatischa, D., Ezziani, A., 2008. An unsplit convolutional perfectly matched layer improved at grazing incidence for the seismic wave equation in poroelastic media. Geophysics 73, 51–61. https://doi.org/10.1190/1.2757586.
Martin, R., Komatitsch, D., Gedney, S.D., Bruthiaux, E., 2010. A high order time and space formulation of the unsplit perfectly matched layer for the seismic wave equation using auxiliary differential equations (ADEPML). Comput. Model. Eng. Sci. 56 (1), 17–42.
Martin, R., Bodet, L., Tournat, V., Rejiba, F., 2019. Seismic wave propagation in nonlinear viscoelastic media using the auxiliary differential equation method. Geophys. J. Int. 216, 453–469.
Maxwell, J.C., 1867. On the dynamical theory of gases. Phil. Trans. Roy. Soc. Lond. 157, 49–88.
Murphy, W.F., 1982. Effects of microstructure and pore fluids on the acoustic properties of granular sedimentary materials (PhD. Stanford University).
Ramadan, O., 2003. Auxiliary differential equation formulation: an efficient implementation of the perfectly matched layer. IEEE Microw. Wireless Compon. Lett. 13, 69–71. https://doi.org/10.1109/LMWC.2003.808706.
Robertsson, J.O., Blanch, J.O., Symes, W.W., 1994. Viscoelastic finite difference modeling. Geophysics 59, 1444–1456. https://doi.org/10.1190/1.1443701.
Roden, J.A., Gedney, S.D., 2000. Convolutional PML (CPML): an efficient FDTD implementation of the CFS-PML for arbitrary media. Microw. Opt. Technol. Lett. 27, 334–339.
Spencer Jr., J.W., 1981. Stress relaxations at low frequencies in fluid-saturated rocks: attenuation and modulus dispersion. J. Geophys. Res. 86, 1803–1812.
Teixeira, F.L., Chew, W.C., 1999. On causality and dynamic stability of perfectly matched layers for FDTD simulations. IEEE Trans. Microw. Theor. Tech. 47, 775–785. https://doi.org/10.1109/22.769350.
Treeby, B.E., Cox, B., 2010. Modeling power law absorption and dispersion for acoustic propagation using the fractional Laplacian. J. Acoust. Soc. Am. 127, 2741–2748. https://doi.org/10.1121/1.3377056.
Virieux, J., 1986. P-SV wave propagation in heterogeneous media; velocity-stress finite-difference method. Geophysics 51, 889–901. https://doi.org/10.1190/1.1442147.
Wang, T., Tang, X.M., 2003. Finite-difference modeling of elastic wave propagation: a nonsplitting perfectly matched layer approach. Geophysics 68, 1749–1755. https://doi.org/10.1190/1.1620648.
White, R.E., 1992. The accuracy of estimating Q from seismic data. Geophysics 57, 1508–1511. https://doi.org/10.1190/1.1443218.
Wuenschel, P.C., 1965. Dispersive body waves; an experimental study. Geophysics 30, 539–551. https://doi.org/10.1190/1.1439620.
Zener, C., 1948. Elasticity and Anelasticity of Metals. University of Chicago Press, Chicago.
Zeng, Y., He, J., Liu, Q.H., 2001. The application of the perfectly matched layer in numerical modeling of wave propagation in poroelastic media. Geophysics 66, 1258–1266. https://doi.org/10.1190/1.1487073.
Zhang, W., Shen, Y., 2010. Unsplit complex frequency-shifted PML implementation using auxiliary differential equation for seismic wave modeling. Geophysics 75, T141–T154. https://doi.org/10.1190/1.3463431.
Zhu, T., Carcione, J.M., 2014. Theory and modelling of constant-Q P and S-waves using fractional spatial derivatives. Geophys. J. Int. 196, 1787–1795.
Zhu, T., Harris, J.M., 2014. Modeling acoustic wave propagation in heterogeneous attenuating media using decoupled fractional Laplacians. Geophysics 79, T105–T116. https://doi.org/10.1190/geo2013-0245.1.